Title:
Advanced CAD Modeling Techniques for Electrospun Membranes: Employing fractal Dimension Optimization for Enhanced Precision

Authors:
Mingdai Yang, mingdai@yu.ac.kr, Yeungnam University
Shuo Chen, 22250068@yu.ac.kr, Yeungnam University
Hanwei Teng, 19508068860thw@yu.ac.kr, Yeungnam University
Taejo Ko, tjko@yu.ac.kr, Yeungnam University

Keywords:
Fractal Dimension, Electrospun Membrane, Computer-Aided Design (CAD), Long Fiber Networks, Random fiber network

DOI: 10.14733/cadconfP.2024.136-140

Introduction:

Electrospinning, a process where a polymer-charged solution is stretched in an electrostatic field, yields continuous fibers whose diameters vary from tens of nanometers to several microns. This technique finds broad application in various domains, including tissue engineering, electrochemical devices, drug delivery, and secondary batteries, due to its versatility and effectiveness [1-5]. While these products appear as continuous sheets at a macro level, their mesoscopic modeling is crucial as their properties are intricately linked to both the fiber characteristics and the network of fibers [6,7].

However, existing models in this domain often fall short of capturing the inherent randomness of these structures, which manifests at multiple scales, such as in irregularities. To address this, the concept of fractal dimensions comes into play, offering a quantitative method to describe these random, complex, and highly irregular scales [8]. In porous media modeling, the fractal dimension typically pertains to surface topography [9], a factor deeply intertwined with the material's performance [10].

To advance this field, a novel modeling method has been introduced. This approach employs a genetic algorithm to optimize fiber arrangement, thereby achieving the desired fractal dimensions. It integrates 2D porosity derived from image analysis with 3D porosity from experimental data, ensuring a comprehensive control of the reconstructed model. Moreover, this method not only fine-tunes fiber placement but also adjusts pore shape and size distribution. As a result, a robust computer-aided design (CAD) model of the electrospun membrane featuring realistic thickness has been successfully constructed using ABAQUS software based on the 2D model.

Main Idea:

Figure 1 illustrates the electrospinning process. As depicted in Figures 1(a) and 1(b), the material was first dissolved in a DMF solution and then subjected to magnetic stirring at 50°C for six hours. As shown in Figure 1(c), upon cooling the solution to room temperature, it was extruded through a syringe, stretched under a high-voltage electrostatic field, and finally collected on a roller.

Poly(vinylidene fluoride co-hexafluoropropylene) (PVDF-HFP, Mw=400 000), poly(PMMA, 120 000), and N,N-dimethylformamide (DMF, anhydrous, 99.8%) were procured from Sigma-Aldrich (St. Louis, MO 63103). All these materials are used as received. The morphology of the separator is examined by field emission SEM (FE-SEM/EDS S-4800, Hitachi Ltd.). The imaging uses high voltage, high current, and lower probes to highlight the mesostructure of the fiber network surface.

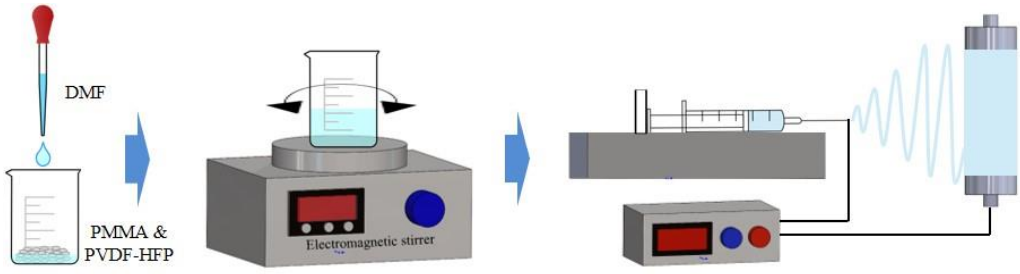

Fig. 1: Process of electrospinning. (a) Solution preparation; (b) solution stirring; and (c) electrospinning.

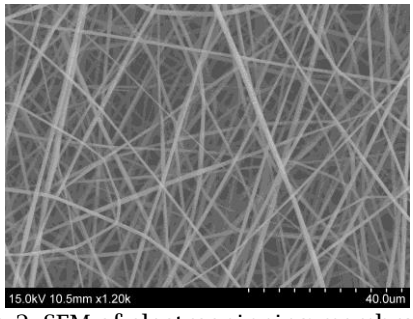

Fig. 2: SEM of electrospinning membrane.

2D modeling

Initially, image analysis was employed to acquire a comprehensive distribution of key sample characteristics, including diameter, orientation, porosity, and fractal dimension, along with volume fractions determined through experimental analysis. Subsequently, leveraging a novel optimization training technique, a two-dimensional representative meta-model was constructed, effectively encapsulating these essential parameters. This approach ensured a harmonized scale of randomness, aligning the model closely with the physical object's attributes.

Utilizing the dataset created through inverse sampling of feature data, fiber groups were synthesized and arranged within a square plane in MATLAB. The model's domain was structured as a 2L × 2L square, encompassing a central L × L black square target area, as illustrated in Figure 3. The model also featured four blue angular regions, designated as the initial movement areas for the fiber starting points. These points are confined to their respective regions, and their movements are dictated by the initial orientation of the fibers. The underlying correspondence is outlined as follows: A(-45°<θ <45°), B(45°<θ<135°), C(135°<θ<180° or -180°<θ<-135°), and D(135°<θ<-45°).

Fibers are translated through changes in their starting point coordinates, thereby adjusting the arrangement of the fibers. Let the number of fibers be n and the coordinates of the initial ends of the fibers (x_i, y_i) be

$$(x_i, y_i) = (x_0 + \nabla x, y_0 + \nabla y) \qquad 0 < i \le n, i \in N \tag{1}$$

where (x_0, y_0) is the initial value of the fiber coordinates, which is one of the following vertex coordinates: A(0,L), B(L,0), C(2L,L), and D(L,2L). $(\nabla x, \nabla y)$ is the fiber coordinate increment. Specifically, the movement area of the starting point of the fiber is limited. Therefore, the coordinates of the starting point can be simplified according to the angular area where it is located.

Vector $X = [\nabla x_1, \nabla y_1, \ldots, \nabla x_i, \nabla y_i, \ldots, \nabla x_n, \nabla y_n]$, $X \in (0,1)$ was set as $[X_1, X_2, \ldots, X_{2n}]$. The coordinates of the fiber starting point (x_i, y_i) in different angular regions are as follows [11]:

$$\begin{cases} x_i = 0 + 0.5LX_{2i-1} \\ y_i = L + |x_i|(2X_{2i} - 1) \end{cases} (x_i, y_i) \in A \quad \begin{cases} y_i = L + 0.5LX_{2i} \\ x_i = 0 + |y_i|(2X_{2i-1} - 1) \end{cases} (x_i, y_i) \in B$$

$$\begin{cases} x_i = 2L - 0.5LX_{2i-1} \\ y_i = L + |x_i|(2X_{2i} - 1) \end{cases} (x_i, y_i) \in C \quad \begin{cases} y_i = L - 0.5LX_{2i} \\ x_i = 2L + |y_i|(2X_{2i-1} - 1) \end{cases} (x_i, y_i) \in D \qquad (2)$$

where ΔA, ΔB, ΔC, and ΔD refer to the triangle area where points A, B, C, and D are located, respectively. The translation of each fiber can be realized by adjusting the size of each sub-item in the vector X.

Three parameters are optimized: porosity, volume fraction, and fractal dimension. Owing to the close correlation between the latter two, the parameters can be simplified using a weighted combination:

$$\begin{cases} Obj(1) = |(por + vol) - (obj_{por} + obj_{vol})| \le 0.01 \\ Obj(2) = |frac - obj_{frac}| \le 0.01 \end{cases} \qquad (3)$$

where *por*, *vol*, and *frac* are the target values obtained from experiments/graphical analysis, which are porosity, volume fraction, and fractal dimension. The target fractal dimension is the average of multiple fractal dimensions of the sample. obj_{por}, obj_{vol}, and obj_{frac} are the corresponding values of the current model. Owing to numerical errors in the optimization objective, 0.01 was set as an acceptable target convergence value.

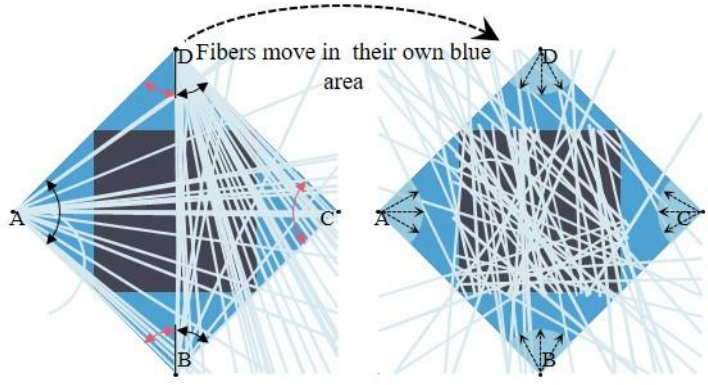

Fig. 3: 2D modeling method of electrospun membrane [11].

3D modeling

The coordinate data from the 2D MATLAB model were transferred into ABAQUS software to construct a three-dimensional fiber layer model. By integrating multiple distinct 3D fiber layer models, a solid CAD model of the electrospun membrane, complete with a realistic thickness, was created. This mirrors the electrospinning formation mechanism, where a nonwoven structure emerges through layered spinning.

The diameter and coordinate data of each fiber in the MATLAB 2D model's target area were exported to a text file. Subsequently, a custom Python script was utilized within ABAQUS's script module to facilitate modeling. In the model, each fiber and the compressor plane were fixed in all directions except along the z-axis, preventing lateral drift. The compressor plane dynamically advanced towards the collector plane in finite element simulations. During this movement, the fibers stacked upon each other and underwent continuous compression. This process persisted until the fiber layer's thickness was reduced to the SEM imaging depth, h. The resulting deformed mesh represents a 3D fiber network layer model.

In this way, multiple 3D representative fiber layers, each 10 μm thick, were generated. These compressed layers were imported into Abaqus as individual components. The layers were sequentially arranged and combined, mirroring the thickness of typical electrospun membranes, which ranges from 70 to 80 μm. Consequently, eight 3D fiber layers were selected to construct a solid CAD model of an electrospun membrane with an 80 μm thickness. This model comprises 608 long fibers, emulating the experimental process of stacking spun fibers to create electrospun membranes.

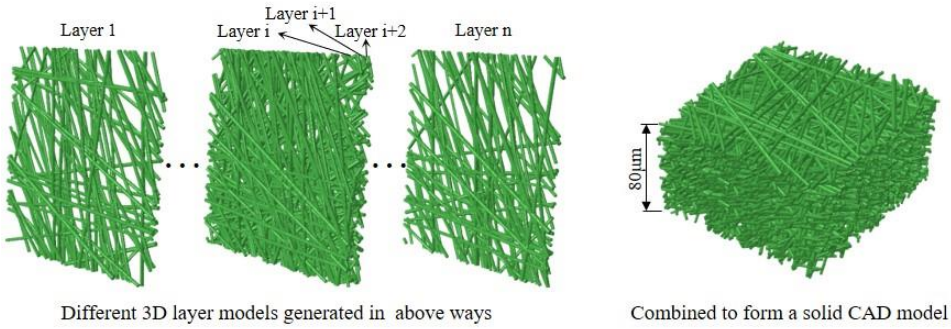

Fig. 4: 3D modeling method of electrospun membrane [11].

Conclusions:

Leveraging the newly developed model and optimization technique, key parameters such as the fractal dimension of the 2D model can now be manipulated with enhanced speed and precision. This approach facilitates a precise alignment between the fiber network model and the randomness scale observed in physical objects.

In alignment with the intrinsic formation mechanisms of electrospun membranes, this innovative methodology for constructing 3D models adeptly captures the attributes of realistic thickness. This advancement not only mirrors the natural process but also introduces a level of accuracy and control previously unattainable in such modeling.

Acknowledgements:

This work was supported by the National Research Foundation of Korea (NRF) grant funded by the Korean government (MSIT) (RS-2023-00278890).

References:

[1] Xue, J.; Wu, T.; Dai, Y.; Younan Xia, Y.: Electrospinning and Electrospun Nanofibers: Methods, Materials, and Applications. Chemical Reviews, 119(8), 2019, 5298-5415. https://doi.org/10.1021/acs.chemrev.8b00593

[2] Rahmati, M.; Mills, D. K.; Urbanska, A. M.; MSaeb, M. R.; Venugopal, J. R.; Ramakrishna, S.; Mozafari, M.: Electrospinning for tissue engineering applications, Progress in Materials Science, https://doi.org/10.1016/j.pmatsci.2020.11.014

[3] Wang, H.-G.; et al.: Electrospun materials for lithium and sodium rechargeable batteries: from structure evolution to electrochemical performance, Energy & Environmental Science, 8.6, 2015, 1660-1681. https://doi.org/10.1039/C4EE03912B

[4] Luraghi, A.; Peri, F.; Moroni, L.: Electrospinning for drug delivery applications: A review, Journal of Controlled Release, 334, 2021, 463-484, https://doi.org/10.1016/j.jconrel.2021.03.033

[5] Ji-Won, J.; et al.: Electrospun nanofibers as a platform for advanced secondary batteries: a comprehensive review, Journal of Materials Chemistry A 4.3, 2016, 703-750. https://doi.org/10.1039/C5TA06844D

[6] Ting, D.; et al.: Surface-modified electrospun polyacrylonitrile nano-membrane for a lithium-ion battery separator based on phase separation mechanism, Chemical Engineering Journal 398, 2020, 125646. https://doi.org/10.1016/j.cej.2020.125646
[7] Leng, X.; Yang, M.; Li, C.; UI Arifeen, W.; Ko, T. J.: High-performance separator for lithium-ion battery based on dual-hybridizing of materials and processes, Chemical Engineering Journal, 2021, 133773, https://doi.org/10.1016/j.cej.2021.133773
[8] Mandelbrot, B. B.: The fractal geometry of nature. Vol. 1. New York: WH freeman, 1982.
[9] Mahjani, M. G.; Moshrefi, R.; Sharifi-Viand, A.; Taherzad, A.; Jafarian, M.; Hasanlou, F.; Hosseini, M.: Surface investigation by electrochemical methods and application of chaos theory and fractal geometry, Chaos, Solitons & Fractals, 91, 2016, 598-603, https://doi.org/10.1016/j.chaos.2016.08.011
[10] Yu, Q.; et al.: Estimation of sandstone permeability with SEM images based on fractal theory, Transport in Porous Media 126, 2019, 701-712. https://doi.org/10.1007/s11242-018-1167-2.
[11] Yang, M.-D.; Leng, X.-L.; Ko, T. J.: CAD Modeling method of the electrospun membrane under multifractal dimension optimization control, Chaos 1 June 2023; 33(6), 063129. https://doi.org/10.1063/5.0151528